Transmission function of the collinear acousto-optical filter controlled by acoustic waves of the finite amplitude

Alexandre S. Shcherbakov
Adán Omar Arellanes
Sergey A. Nemov

Transmission function of the collinear acousto-optical filter controlled by acoustic waves of the finite amplitude

Alexandre S. Shcherbakov
Adán Omar Arellanes
National Institute for Astrophysics, Optics &
    Electronics (INAOE)
Puebla 72000, Mexico
E-mail: arellaneso@inaoep.mx

Sergey A. Nemov
St. Petersburg State Polytechnic University
Polytechnicheskaya Street 29
St. Petersburg 195251, Russian Federation

Abstract. An opportunity to exploit specific mechanisms of the acousto-optic nonlinearity to regulate performances of the collinear acousto-optical filter, realizing the sequential spectrum analysis of optical signals, is considered. This possibility is theoretically analyzed and experimentally confirmed with an advanced filter based on calcium molybdate ($CaMoO_4$) single-crystal with a 15-μs time-aperture. It is able to operate over red and near-infrared light at relatively low radio-wave frequencies providing almost lossless regime for controlling acoustic waves of the finite amplitude. Under certain conditions, the transmission function of electronically tunable filter exhibits a marked dependence on the applied acoustic power density, and as a result, one can significantly squeeze the transmission function, i.e., improve the spectral resolution of this filter at the cost of decreasing the efficiency of the device partially. The identified and observed non-linear effect makes possible varying the performance data of similar advanced collinear acousto-optical filter governed by external signals of the finite amplitude. © *2013 Society of Photo-Optical Instrumentation Engineers (SPIE)* [DOI: 10.1117/1.OE.52.6.064001]

Subject terms: collinear acousto-optical interaction; optical filter; acousto-optical nonlinearity; transmission function; spectral resolution; waves of the finite amplitude.

Paper 130240 received Feb. 11, 2013; revised manuscript received Apr. 14, 2013; accepted for publication May 7, 2013; published online Jun. 10, 2013.

1 Introduction

In 1970s to 1980s, novel optical spectral devices, electronically tunable acousto-optical filters (AOF) had been proposed and developed. As the years passed by, the AOFs have been remarkably progressed, and now they are widely exploited, for example, in modern astrophysical observations.[1,2] Schematically, the AOF can be separated on collinear and non-collinear filters, depending on the relative directions of passing the waves through crystalline cell within their geometric arrangements, as well as on sequential and parallel devices, depending on the algorithms realizing the spectrum analysis of optical signals. Their features are characterized by the amplitude and spectral parameters. Collinear acousto-optical interaction by itself had been initially predicted and studied in the middle of 1960s by R.W. Dixon,[3] and then in the 1970s it has been exploited in various applications, among which first of all one ought to call the collinear tunable acousto-optical filters.[4–8] The conventional analysis of this phenomenon in terms of lossless plane waves was presented in a number of classical issues.[9,10] Practically, the methods of acousto-optics had manifested themselves as rather effective due to their property of quantum mechanic amplification resulting in the control over high-energetic photons by low-energetic phonons. The corresponding gain is represented by the direct ratio of the scattered photon frequency to a frequency of the controlling phonon frequency. It allows practical application of a given acoustic field approximation or the regime of a weak coupling, when the spatial distribution of acoustic beam is almost independent on the spatial distribution of light that

leads to considerable theoretical and practical facilities. In particular, 100% efficiency of light scattering may be achieved without any effect on the acoustic beam, so the above-mentioned control can be repeated a lot of times with low losses of acoustic energy. Moreover, an essential difference between velocities of light and ultrasound gives us an opportunity for applying the quasi-stationary approximation to the analysis of modern acousto-optical problems. In the past decades, great progress has been made in acousto-optics, and now, it is a widely used technique in the field of data processing.[11] Nevertheless, recently the existence of a new branch in studies and applications of collinear acousto-optical interaction, which is associated with acousto-optical nonlinearity, for example, in the form of three-wave coupled states, has been manifested.[12,13] That is why we believe that it is a worthwhile investment to further develop this line because the objects being under consideration here are closely connected with the above-mentioned nonlinearity in the regime of a weak coupling. With this consideration, we develop the exact and closed analytical model of the collinear light scattering by continuous acoustic waves of the finite amplitude in a birefringent lossless material. Similar approach definitely includes practically important case of the presence of really small acoustic attenuation in widely used acousto-optical filters operating in the traveling-wave regime at relatively low radio-frequency acoustic waves and exploiting such materials as α–quartz or calcium molybdate single crystals. In doing so, we analyze the peculiarities of the effect conditioned by the acousto-optical nonlinearity, which leads to a measurable dependence of the transmission function, and consequently, the spectral resolution peculiar to this filter on the applied power density of acoustic waves of the finite

amplitude in a way allowing, for instance, to improve the spectral resolution of similar device at the cost of partial demerit for the filter efficiency.

2 Three-Wave Collinear Interaction with the Phase Mismatches

A three-wave co-directional collinear interaction with the mismatched wave numbers in a two-mode lossless medium is described by a set of three nonlinear partial differential equations. Here, we consider the regime of a weak coupling,[12,13] when two light modes are scattered by relatively slow wave, being non-optical by its nature, when essentially effective Bragg scattering of light can be achieved without any observable influence of the scattering process on that non-optical wave because the number of interacting photons is a few orders less than the number of the scattering quanta injected into a medium. Then, the velocities of light modes can be approximated by the same value c, because usually the length of crystalline materials does not exceed 20 cm. In this regime, the above-mentioned set of equations falls into an independent equation for the complex amplitude $U(x, t)$ of a slow wave (V is the velocity of this wave) and a pair of the combined equations for the complex amplitudes $C_0(x, t)$ and $C_1(x, t)$ of the incident (pumping) light wave and scattered one, respectively,

$$\frac{\partial U}{\partial x} + \frac{1}{V}\frac{\partial U}{\partial t} = 0 \tag{1a}$$

$$\frac{\partial C_0}{\partial x} + \frac{1}{c}\frac{\partial C_0}{\partial t} = -q_1 C_1 U * \exp(2i\eta x) \tag{1b}$$

$$\frac{\partial C_1}{\partial x} + \frac{1}{c}\frac{\partial C_1}{\partial t} = q_0 C_0 U \exp(-2i\eta x). \tag{1c}$$

Here, $q_{0,1}$ are the constants of interaction and 2η is the mismatch of wave numbers inherent in the interacting light waves. Now, we go to the tracking coordinates $(x, \tau = t - x/c)$ and assume that non-optical wave, governed by Eq. (1a) and described by $U = u[x(1 - V/c) - V\tau]$ $\exp(i\varphi)$, has the constant phase φ, so that one can convert Eqs. (1b) and (1c) into equations of the second order

$$\frac{\partial^2 C_{0,1}}{\partial x^2} - \left(\frac{1}{u}\frac{\partial u}{\partial x} \pm 2i\eta\right)\frac{\partial C_{0,1}}{\partial x} + q_0 q_1 u^2 C_{0,1} = 0. \tag{2}$$

We put $C_{0,1} = a_{0,1}(x, t)\exp[i\Phi_{0,1}(x, t)]$, $\gamma_{0,1} = \partial\Phi_{0,1}/\partial x$ and then divide real and imaginary parts in Eq. (2) as

$$\frac{\partial^2 a_{0,1}}{\partial x^2} - \frac{1}{u}\frac{\partial u}{\partial x}\frac{\partial a_{0,1}}{\partial x} + [q_0 q_1 u^2 - \gamma_{0,1}^2 \pm 2\eta\gamma_{0,1}]a_{0,1} = 0, \tag{3}$$

$$2(\gamma_{0,1}\mp\eta)\frac{\partial a_{0,1}}{\partial x} + \left(\frac{\partial\gamma_{0,1}}{\partial x} - \frac{\gamma_{0,1}}{u}\frac{\partial u}{\partial x}\right)a_{0,1} = 0. \tag{4}$$

Equation (4) has the following general solutions

$$\gamma_{0,1} = \pm\eta u a_{0,1}^{-2}\int u^{-1}(\partial a_{0,1}^2/\partial x)\mathrm{d}x + \Gamma_{0,1} u a_{0,1}^{-2}, \tag{5}$$

where $\Gamma_{0,1}$ are the integration constants. The analysis shows that the collinear light scattering with $\Gamma_{0,1} \neq 0$ leads to

appearing optical backgrounds. After further analysis here, the only regime with $\Gamma_{0,1} = 0$ will be considered in a view of potential application to filter optical beams without backgrounds.

3 Quasi-Stationary Background-Free Continuous-Wave Regime

Choosing the simplest case of $\Gamma_{0,1} = 0$ in Eq. (5), one can study the phenomenon in the continuous-wave regime for both the incident light and the non-optical wave when $u[x(1 - V/c) - V\tau] = U_0$ is constant. Equations (3) and (4) are analyzed with the fixed magnitude of the mismatch η and natural for practice the boundary conditions $a_0(x = 0, t) = 1$, $(\partial a_0/\partial x)(x = 0, t) = 0$, $a_1(x = 0, t) = 0$, $(\partial a_1/\partial x)(x = 0, t) = q_0 U_0$ in a half-infinite medium. In so doing, one yields $\gamma_{0,1} = \pm\eta$ and $-\gamma_{0,1}^2 \pm 2\eta\gamma_{0,1} = \eta^2$. Thus, with the parameter $q_0 q_1 U_0^2 = \sigma^2$, characterizing physical contributions of both the material properties and the power density of non-optical wave, Eq. (3) takes the form

$$\frac{\partial^2 a_{0,1}}{\partial x^2} + (\sigma^2 + \eta^2)a_{0,1} = 0. \tag{6}$$

To construct the solution, which can be easily used in practically important cases of significant phase mismatches, we use the conservation law $q_0 a_0^2 + q_1 a_1^2 = q_0$–const, resulting from Eq. (1b) and (1c). Combining Eq. (6) for a_0 and a_1, one can obtain a pair of the following equations:

$$\frac{\partial(a_{0,1}^2)}{\partial x} = 2\sqrt{a_{0,1}^2(q_{0,1}^{-1}q_0 - a_{0,1}^2)(\sigma^2 + \eta^2)}, \tag{7}$$

whose solutions with arbitrary integration constants $\theta_{0,1}$ are given by

$$a_{0,1}^2 = q_{0,1}^{-1}q_0 \sin^2[\theta_{0,1} + G(x)] \tag{8a}$$

$$G(x) = x\sqrt{\sigma^2 + \eta^2}. \tag{8b}$$

Using the above-noted boundary conditions, one arrives at

$$\theta_0 = \arcsin\left[\sigma^{-1}\sqrt{\sigma^2 + \eta^2}\right] \tag{9a}$$

$$\theta_1 = 0, \tag{9b}$$

so that the stationary intensities of the pumping and scattered light waves can be expressed as

$$|C_0(x)|^2 = \frac{\eta^2}{\sigma^2 + \eta^2} + \frac{\sigma^2}{\sigma^2 + \eta^2}\cos^2[G(x)] \tag{10a}$$

$$|C_1(x)|^2 = \frac{q_0}{q_1}\frac{\sigma^2}{\sigma^2 + \eta^2}\sin^2[G(x)]. \tag{10b}$$

These solutions include contributions of two types. The first summand in the intensity $|C_0|^2$ represents a background determined by the mismatch η; the second one gives the oscillations imposed on that background. The scattered light wave contains only oscillations without a background due to the above-chosen restriction $\Gamma_{0,1} = 0$.

4 Resolution of CaMoO$_4$ Collinear Filter with the Finite Amplitude Shear Acoustic Wave Signal

4.1 Traditional Approach to the Frequency Resolution

It is well known that the spectral resolution $\delta\lambda$ and the frequency resolution δf of collinear acousto-optical filters are usually estimated as $|\delta\lambda| = (\lambda/f_0)\delta f$ and $\delta f = V/L$, where f_0 and V are the carrier frequency and velocity of acoustic wave; L is the longitudinal aperture of filter, i.e., the length of acousto-optical interaction. It is obviously seen that these formulas do not include potential influence of the initial acoustic power density on the resolution.

At first, let us consider Eqs. (8b) and (10b) for the lossless medium in the case of infinitely small signals, i.e., with $\sigma \to 0$. In so doing, one can estimate $G(x) = \eta x$, $G(0) = 0$, and write

$$|C_1(x)|^2 = \left(\frac{q_0(\sigma x)^2}{q_1}\right) \cdot \frac{\sin^2(\eta x)}{(\eta x)^2}, \quad (11)$$

where the distance x can be considered as a parameter. Historically, estimating the resolution is connected with the well-known Rayleigh criterion, which predicts in fact separating a pair of the neighboring $(\sin u/u)^2$—shaped distributions at the intensity level of $\nu \approx 0.4055$. This is exactly the case of Eq. (11), and one has to resolve the transcendent algebraic equation $\sin(\eta x) = \nu^{1/2}(\eta x) \approx 0.6368(\eta x)$. The first (both positive and negative) solution to this algebraic equations is $\eta_{(\pm)}x = \pm\pi/2$. This gives us the bandwidth from $\eta_{(-)}x = -\pi/2$ to $\eta_{(+)}x = +\pi/2$, i.e., to the full bandwidth at the intensity level: $\nu \approx 0.4055$ $\Delta\eta x = \eta_{(-)}x + \eta_{(+)}x = |-\pi/2| + |+\pi/2| = \pi$. Together with this a one-side mismatch η had been previously [see Eq. (1b) and (1c)] determined as $\eta = \Delta K/2 = \pi\delta f/V$, so that in the more detailed form $\eta_{(\pm)} = \pi\delta f_{(\pm)}/V$ (where $\delta f_{(\pm)}$ are the corresponding one-side frequency deviations) and consequently, the total deviation of the mismatch is given by $\Delta\eta = \eta_{(-)} + \eta_{(+)} = \pi(\delta f_{(-)} + \delta f_{(+)})/V = \pi\delta f/V$. Combining the expressions, which includes $\Delta\eta$, one arrives at the above-noted formula $\delta f = V/x$, where one can undoubtedly put $x = L$. Thus, one can see that full width of the main lobe inherent in a $(\sin u/u)^2$—shaped distribution at the intensity level $\nu \approx 0.4055$ gives the "standard" determination of the

frequency resolution in acousto-optics, which is conditioned by the limit $\sigma \to 0$.

4.2 Frequency Resolution for Signals of Finite Amplitude in a Lossless Medium

Now, let us consider Eqs. (8b) and (10b) in the lossless case with signals of the finite amplitude when $\sigma \neq 0$. Because of $G(x) = x\sqrt{\sigma^2 + \eta^2}$ and $G(0) = 0$, one can write

$$|C_1|^2 = \left(\frac{q_0}{q_1}\right) \frac{(\sigma x)^2}{(\sigma x)^2 + (\eta x)^2} \sin^2\left[\sqrt{(\sigma x)^2 + (\eta x)^2}\right]. \quad (12)$$

To estimate the frequency resolution at the above-noted intensity level $\nu \approx 0.4055$ Eq. (12) has to be normalized as

$$\frac{|C_1|^2}{|C_1(\eta=0)|^2} = \left[\frac{(\sigma x)^2}{(\sigma x)^2 + (\eta x)^2}\right] \cdot \frac{\sin^2\left[\sqrt{(\sigma x)^2 + (\eta x)^2}\right]}{\sin^2(\sigma x)}. \quad (13)$$

The 3-D plots inherent in these distributions are presented in Fig. 1 for the scattered light intensity $|C_1(x)|^2$ in absolute units, see Eq. (12), and for the normalized intensity from Eq. (13) in practically reasonable approximation $q_0/q_1 \approx 1$. Figure 1(a) gets the interval $0 \leq \sigma x < 3\pi$ and illustrates a regular structure in absolute units, which exhibits reaching a sequence of unit-valued maxima along the line $\eta x = 0$ with a dimensionless period $\sigma x = \pi$. Figure 1(b) reflects the normalized distribution on the smaller interval $0 \leq \sigma x \leq \pi$ and includes the level $\nu \approx 0.4055$-plane for estimating the width in terms of a one-side dimensionless mismatch ηx.

A set of 2-D plots for the scattered light intensity $|C_1(\sigma x), (\eta x)|^2$ is presented in Fig. 2 in the absolute form for the range of products $1.0 \leq \sigma x < \pi$ in the same approximation $q_0/q_1 \approx 1$. These 2-D plots illustrate in detail the dynamics of evolving the distributions step-by-step and confirm that one can expect narrowing the normalized intensity profile noted by Eq. (13) with $\sigma x \to \pi$ from smaller values as depicted in Fig. 1(b).

With $1.0 \leq \sigma x < \pi$, estimations at the above-chosen intensity level $\nu \approx 0.4055$ give one-side mismatches $\eta x(\sigma x = 1.0) = 1.511$, $\eta x(\sigma x = \pi/2) = 1.414$, $\eta x(\sigma x = 2.0) = 1.292$, $\eta x(\sigma x = 2.5) = 1.059$, and $\eta x(\sigma x = 3.0) = 0.524$, see Fig. 2(b), which lead to the corresponding full
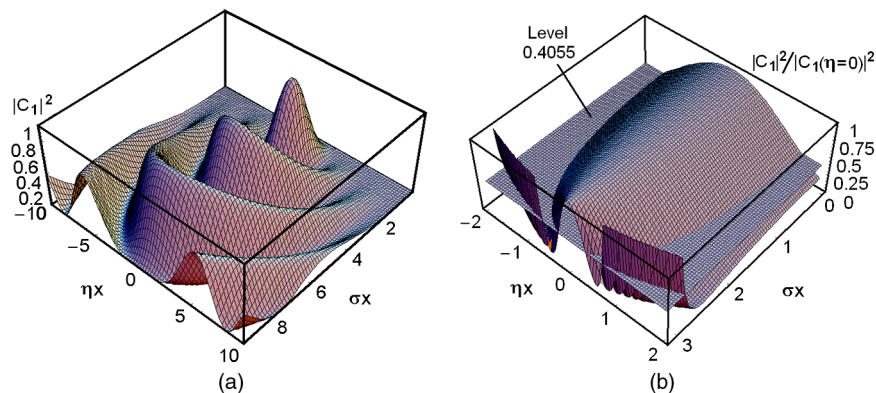

Fig. 1 The 3-D plots of the scattered light intensity profile with $q_0/q_1 \approx 1$: (a) for the absolute values on the interval $0 \leq \sigma x < 3\pi$ and (b) for the normalized distribution on the interval $0 \leq \sigma x \leq \pi$.
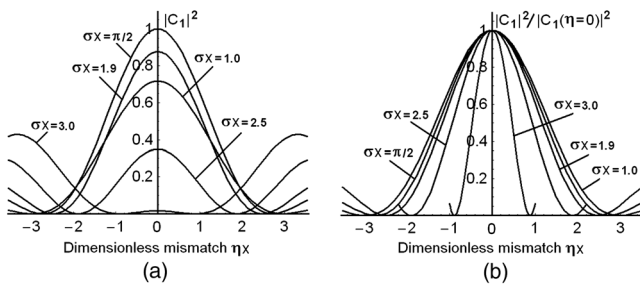
Fig. 2 The 2-D plots $|C_1[(\sigma x),(\eta x)]|^2$ for the products $1.0 \leq \sigma x < \pi$ with $q_0/q_1 \approx 1$: (a) for the absolute values and (b) after normalization by the zero magnitudes.

Fig. 5 The 2-D plots for the products $\pi < \sigma x < 2\pi$ with $q_0/q_1 \approx 1$: (a) for the absolute values and (b) after normalization by the zero magnitudes.

bandwidths $\Delta \eta x(\sigma x) = 2\eta x(\sigma x)$. These numbers should be compared with the previously obtained a one-side mismatch estimation $\eta x(\sigma x \to 0) = \pi/2 \approx 1.5708$ and the full bandwidth $\Delta \eta x(\sigma x \to 0) = \pi$, corresponding to a relatively low efficiency of light scattering in the regime of a given incident optical field approximation. One can see from these estimations and Fig. 2 that the contribution from acoustic wave of the finite amplitude narrows the profiles, and the most efficient regime, providing theoretically 100% efficiency of light scattering, can be achieved with $\sigma x = \pi/2$, see Fig. 2(a), when the profile width will be about 10% better than in the case of a low-power non-optical wave. Growing the product σx makes it possible to narrow profile for more, but at the cost of decreasing the efficiency significantly, see Fig. 3. Nevertheless, a desirable balance between the contour width and efficiency can be found here, for instance, in vicinity of $\sigma x \cong 2.0$, if the case requires.

Figure 4 represents a 2-D contour plot for the normalized light intensity on the plane $[(\sigma x),(\eta x)]$. The contour lies on the interval $0 \leq \sigma x \leq \pi$ and demonstrates the tendency of
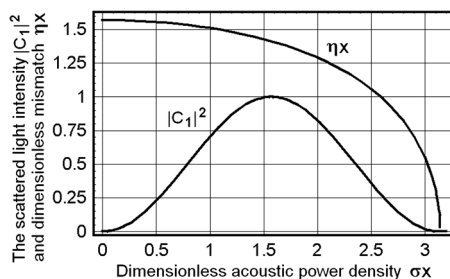
squeezing the normalized light intensity profile with growing the product σx. As a result, one can see that profile width at $\sigma x \to \pi$ is a few times narrower than initial one with $\sigma x \to 0$, i.e., squeezing the transmission function is observed.

Another set of 2-D plots for the normalized scattered light intensity $|C_1[(\sigma x),(\eta x)]|^2 \cdot |C_1(\eta = 0)|^2$ is presented in Fig. 5 for the range of products $\pi < \sigma x < 2\pi$. This range of products σx has not been shown in Fig. 1(b). It is clearly seen from Fig. 5 that the profile width becomes dramatically gained within this range. The most effective case when $|C_1(\eta = 0)|^2 = 1$ is reached at $\sigma x = 3\pi/2$, see Fig. 5(a), but it gives already the profile one-side width $\eta x(\sigma x = 3\pi/2) \approx 2.5$ at the level 0.4055, which is definitely wider than the corresponding profile in the range of products $\pi < \sigma x < 2\pi$.

Figure 6 demonstrates the general tendency to repeat squeezing the profile $|C_1[(\sigma x),(\eta x)]|^2$ periodically, although only the interval $0 \leq \sigma x < 3\pi$ is depicted here. However, the presented 2-D contour plot shows clearly that each next period exhibits a wider profile in the vicinity of the points $\sigma x \to (\pi/2) + m\pi$, $m = 0, 1, 2, 3, \ldots$ related to maximal efficiency of light scattering as well as at the points $\sigma x \to (m + 1)\pi$ of maximal squeezing at this period with the chosen number m. It should be noted that the dynamics of profile transformation within each particular period can be imagined in certain respects by analogy with the plots presented in Figs. 2 and 5 with obvious corrections, of course, for scaling along the ηx-axis. Thus, Fig. 6 makes it possible to conclude that increasing the dimensionless product σx as far as the involved number m growth does not promise any additional squeezing the profile in comparison with the case of $m = 0$.

Fig. 3 The light intensity $|C_1(x)|^2$ and a one-side dimensionless mismatch ηx versus the product σx.
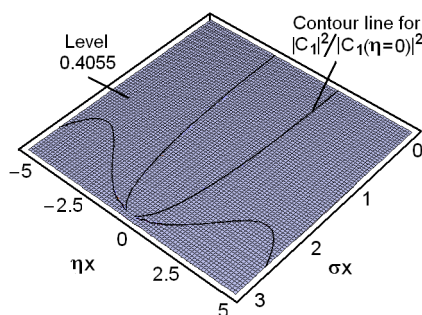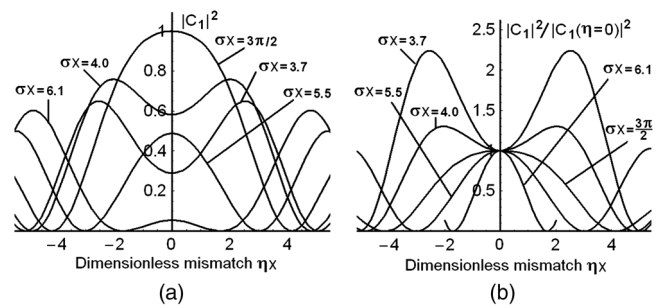

Fig. 4 A 2-D contour for the normalized light intensity on the plane $[(\sigma x),(\eta x)]$ on the interval $0 \leq \sigma x \leq \pi$.
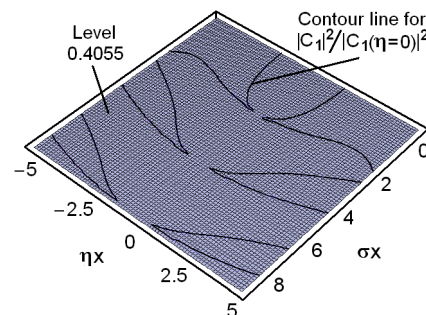

Fig. 6 A 2-D contour plot for the normalized light intensity on the plane $[(\sigma x),(\eta x)]$ on the interval $0 \leq \sigma x < 3\pi$.

5 Efficiency of Collinear Acousto-Optical Interaction in Calcium Molybdate Single Crystal

Now, let us consider a few practically useful estimations related to experimental observation of the collinear acousto-optical interaction with linear acoustic losses in a birefringent cell made of a calcium molybdate (CaMoO$_4$) single crystal. In this particular case, one can observe only anomalous process of light scattering, so that the parameters $q_{0,1}$ are described in Ref. 9 by

$$q_{0,1} = \frac{|\vec{k}_{0,1}|}{4 \, n_{0,1}^2} (\vec{e}_0 \Delta \varepsilon \vec{e}_1).\tag{14}$$

Here, $n_{0,1}$ are the refractive indices for the interacting light waves, $|\vec{k}_{0,1}| = 2\pi n_{0,1}/\lambda$, λ is the light wavelength in a vacuum, and the last term in brackets, describing the efficiency of interaction, is a subject to find. This term includes the eigen-orts $\vec{e}_{0,1}$ of polarizations for the incident and scattered light beams as well as the tensor $\Delta \varepsilon$ of perturbations of the dielectric permittivity under action of the acoustic wave in a medium. To estimate the efficiency of interaction, i.e., to find the contribution of brackets to Eq. (14), we consider the acoustic modes with the wave unit-vector $\vec{m}$ oriented along the [100]-axis, so that $\vec{k}_{0,1} = \vec{m}|\vec{k}_{0,1}|$. In this case, the longitudinal mode gives zero efficiency of interaction due to the symmetry of CaMoO$_4$-crystal, while the contribution from the shear mode with its unit-vector $\vec{u}$ of the transversal elastic displacements oriented along the [001]-axis, i.e., with $\vec{u} = [0, 0, 1]$, has to be calculated. Thus, one can write the deformation tensor γ and the unperturbed dielectric permittivity tensor ε in the main crystallographic axes as

$$\gamma = \frac{\gamma_0}{2}(\vec{u} \cdot \vec{m} + \vec{m} \cdot \vec{u}) = \frac{\gamma_0}{2}\begin{pmatrix} 0 & 0 & 1 \\ 0 & 0 & 0 \\ 1 & 0 & 0 \end{pmatrix}\tag{15a}$$

$$\varepsilon = \begin{pmatrix} \varepsilon_0 & 0 & 0 \\ 0 & \varepsilon_0 & 0 \\ 0 & 0 & \varepsilon_e \end{pmatrix}.\tag{15b}$$

Here, γ_0 is the amplitude of the shear deformation, while $\varepsilon_0 = n_0^2$ and $\varepsilon_e = n_e^2$ are the eigen-values of the unperturbed dielectric permittivity tensor ε. Now, the tensor γ of the second rank with the components γ_{kl} ($k, l = 1, 2, 3$) can be converted into a 6-dimension vector $\bar{\gamma} = \gamma_0(0, 0, 0, 0, 1, 0)$ with the components $\bar{\gamma}_\mu$ ($\mu = 1, \ldots, 6$) using the standard procedure,[14] which includes re-notating $\bar{\gamma}_\mu = \gamma_{kk}$ ($\mu = 1, 2, 3$) and $\bar{\gamma}_\mu = 2\gamma_{kl}$ ($k \neq l, \mu = 4, 5, 6$). Now, if one will use the same procedure[14] and take the photo-elastic tensor p of the fourth rank for a calcium molybdate single crystal in the form of a 6×6 matrix $\hat{p}$, first, it will be allowed to construct and calculate the product $\hat{p}\,\bar{\gamma} = \gamma_0(0, 0, 0, p_{45}, p_{44}, 0)$, and then to convert the result back to the form of a standard tensor $(p\gamma)$ of the second rank.

The next step of our analysis is connected with finding the dielectric permittivity perturbations tensor $\Delta \varepsilon$, whose components can be written as $\Delta \varepsilon_{ij} = \varepsilon_{im}\varepsilon_{nj}p_{mnkl}\gamma_{kl}$.[9] In the particular case of a CaMoO$_4$ crystal whose point symmetry group is 4/m, one can write:[14–16]

$$p_{\lambda\mu} = \begin{pmatrix} p_{11} & p_{12} & p_{13} & 0 & 0 & p_{16} \\ p_{12} & p_{11} & p_{13} & 0 & 0 & -p_{16} \\ p_{31} & p_{31} & p_{33} & 0 & 0 & 0 \\ 0 & 0 & 0 & p_{44} & p_{45} & 0 \\ 0 & 0 & 0 & -p_{45} & p_{44} & 0 \\ p_{61} & -p_{61} & 0 & 0 & 0 & p_{66} \end{pmatrix}$$

$$= \begin{pmatrix} 0.17 & -0.15 & -0.08 & 0 & 0 & 0.03 \\ -0.15 & 0.17 & -0.08 & 0 & 0 & -0.03 \\ 0.10 & 0.10 & 0.08 & 0 & 0 & 0 \\ 0 & 0 & 0 & 0.06 & 0.06 & 0 \\ 0 & 0 & 0 & -0.06 & 0.06 & 0 \\ 0.10 & -0.10 & 0 & 0 & 0 & 0.03 \end{pmatrix}.\tag{16}$$

The result of calculating has the form

$$\Delta \varepsilon = \gamma_0 \varepsilon_0 \varepsilon_e \begin{pmatrix} 0 & 0 & p_{44} \\ 0 & 0 & p_{45} \\ p_{44} & p_{45} & 0 \end{pmatrix}.\tag{17}$$

Now, we take into account the orts $\vec{e}_{0,1}$ of polarization for the incident and scattered light waves. When the wave vectors of these light waves are collinear to the wave normal ort $\vec{m}$ for the acoustic wave and, of course, to the [100]-axis in calcium molybdate crystal, the eigen-orts $\vec{e}_{0,1}$, of light polarizations should be oriented, as it directly follows from Eq. (15b), along the [010] and [001] axes, so that one can take, for example, $\vec{e}_0 = [0, 1, 0]$ and $\vec{e}_1 = [0, 0, 1]$ with $n_0 = n_o$ and $n_1 = n_e$. As a result, one can obtain the contribution of brackets to Eq. (14) as

$$\vec{e}_0 \Delta \varepsilon \vec{e}_1 = \vec{e}_1 \Delta \varepsilon \vec{e}_0 = \gamma_0 \varepsilon_0 \varepsilon_e p_{45}.\tag{18}$$

In doing so, one can find that $q_{0,1} = \pi(2\lambda)^{-1} n_{e,o} \gamma_0 n_{o,e}^2 p_{45}$. One can see that the difference between q_0 and q_1 is rather small because $q_0/q_1 = n_e/n_o$. Then, because the amplitude of deformation can be explained as $\gamma_0 = \sqrt{2P/(\rho V^3)}$, where P is the acoustic power density, one can finally obtain

$$q_0 = \frac{\pi}{\lambda} \sqrt{\frac{P}{2}\left(\frac{n_e^2 n_o^4 p_{45}^2}{\rho V^3}\right)}\tag{19a}$$

$$q_1 = \frac{\pi}{\lambda} \sqrt{\frac{P}{2}\left(\frac{n_o^2 n_e^4 p_{45}^2}{\rho V^3}\right)}.\tag{19b}$$

It should be noted that the factors taken in brackets in Eq. (19a) and (19b) represent the figure of acousto-optical merit peculiar to estimating the efficiency of crystalline materials in acousto-optics,[17] while the refractive indices are slightly dispersive in behavior, see Table 1.

At this step, we are ready to perform a few numerical estimations inherent in the collinear interaction under consideration at the light wavelength of $\lambda = 671$ nm in the CaMoO$_4$-crystalline cell. Taking the material density

Table 1 Dispersion of the main refractive indices n_e and n_o in the calcium molybdate crystal.[18]

λ(nm)	500	600	700	800	900	1000
n_e	2.0239	1.9983	1.9843	1.9781	1.9705	1.9658
n_o	2.0116	1.9884	1.9775	1.9683	1.9634	1.9597

$\rho = 4.34$ g/cm^3, acoustic velocity $V = 2.95 \cdot 10^5$ cm/s, $p_{45} = 0.06$, $n_e = 1.9889$, $n_o = 1.9811$, and $\Delta n = 0.0078$ at the chosen light wavelength,[18] one can calculate the figure of acousto-optic merit $M_2 = n_o^3 n_e^3 p^2 (\rho V^3)^{-1}$, where p is an effective photo-elastic constant, and ρ is the crystal density, as $M_2 \approx 1.977 \cdot 10^{-18}$ (s^3/g) with an accuracy of about 1%.

6 Some Estimations for the Calcium Molybdate Optical Filter

Together with this, one can estimate the potential contributions of the acoustic losses. The coefficient of linear attenuation for the chosen shear acoustic wave passing along the [100]-axis is $\Gamma = 60$(dB/cm GHz^2) in a calcium molybdate single crystal.[18] The factor α of the amplitude acoustic losses measured in cm^{-1} can be expressed via the standard relation: α(cm^{-1}) $= 0.1152 \cdot \Gamma$(dB/cm GHz^2) $\cdot f^2$(GHz). The carrier frequency f_0, peculiar to the collinear acousto-optical interaction in calcium molybdate at the above-mentioned light wavelength 671 nm, can be calculated as $f_0 = \Delta n \cdot V / \lambda \approx 37.3$ MHz, so that one can estimate the amplitude factor of acoustic losses by $\gamma = \Gamma$(dB/cm GHz^2) $\cdot f_0^2$(GHz) ≈ 0.08334(dB/cm) and $\alpha = 0.00962$ cm^{-1}. Due to the smallness of the factors γ and α, one can neglect the effect of acoustic attenuation and consider this case like practically lossless one.
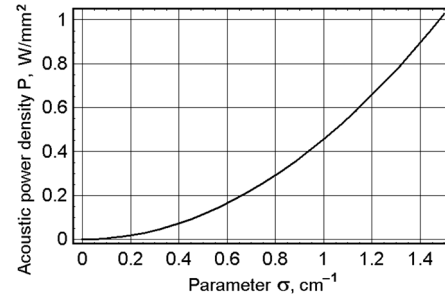
The angular divergence of acoustic beam in a calcium molybdate collinear cell at the frequency $f = 37.3$ MHz can be estimated as well. Practically, a reliable spatial size of the initial acoustic beam aperture that we will consider is close to $d \approx 0.2$ cm. Thus, one can estimate $\Lambda = V/f = 7.91 \cdot 10^{-3}$ cm, and $\varphi = \Lambda/d \approx 3.955 \cdot 10^{-2}$ rad≈ 2.267 deg, and conclude that the angular divergence of acoustic beam can be also omitted. The full mismatch $\Delta\eta$ is connected with the frequency resolution δf. Due to the above-mentioned expression $\Delta\eta = \pi\delta f / V$, one can find $\delta f = (\Delta\eta \cdot x)V/(\pi L)$.

At this step, we are ready to perform a few practical numerical estimations inherent in the collinear interaction at the light wavelength of $\lambda = 671$ nm in the CaMoO$_4$-crystalline cell with $M_2 \approx 1.977 \cdot 10^{-18}$ (s^3/g) and $L = 4.4$ cm. The periodicity of collapsing the resolution (see Fig. 7) is characterized by simple formula $\sigma_m L = m\pi$, so that for a pair of the first periods with $m = 1, 2$ one has $\sigma_1 = \pi/L \approx 0.714$ cm^{-1} and $\sigma_2 = 2\pi/L \approx 1.428$ cm^{-1}.

Using the standard determination introduced above, one can write

$$\sigma = U_0 \sqrt{q_0 q_1} \approx \frac{\pi}{\lambda} \sqrt{\frac{P}{2} M_2} \tag{20a}$$

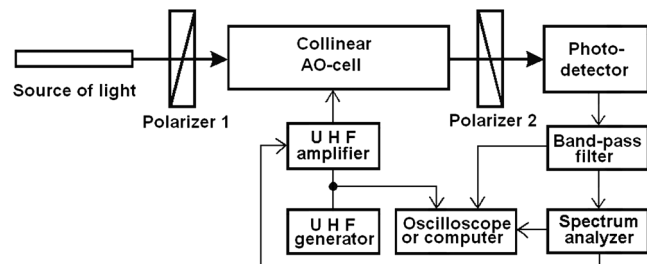$$P \approx \frac{2\lambda^2 \sigma^2}{\pi^2 M_2}. \tag{20b}$$

Fig. 7 Acoustic power density P vs. the parameter σ at $\lambda = 671$ nm in the above-chosen collinear CaMoO$_4$-crystalline cell.

Consequently, Eq. (20b) gives $P[\text{W/mm}^2] \approx 0.457 \cdot (\sigma[\text{cm}^{-1}])^2$, so that $P_1 \approx 0.233[\text{W/mm}^2]$ for σ_1 and $P_2 \approx 0.932[\text{W/mm}^2]$ for σ_2, see Fig. 7. One can see that reaching the second point of collapsing the resolution needs four-times higher acoustic power density in comparison with the first point and looks rather conjectural from the viewpoint of requirements to electric strength inherent in the available piezoelectric transducer. Then, the above presented theoretical 2-D contour plot had shown that each next period exhibits a wider profile in the vicinity of the points $\sigma x \rightarrow (\pi/2) + m\pi$, $m = 0, 1, 2, 3, \ldots$ related to maximal efficiency of light scattering at this period. This is why we have restricted ourselves by reaching the first point of collapsing the resolution in the experiments.

7 Scheme for the Experiments with a Calcium Molybdate Cell

To realize the process of filtering experimentally, we use schematic shown in Fig. 8. It consists of a continuous-wave laser, a CaMoO$_4$-crystalline acousto-optical cell with a pair of the Glan-Thompson crystalline polarizers (with the extinction ratio 10^5 each) whose combined layout is presented in details in Fig. 9, a silicon photo-detector, and a set of electronic equipment for both generating and registering the corresponding electric ultra-high-frequency (UHF) radio-wave signals. Initially, the tunable UHF-signal is applied to the electronic input port of the collinear acousto-optical cell through a wide-band UHF-amplifier HD18858 (10–1000 MHz, 8 W), see Figs. 8 and 9, and to the input of an oscilloscope (or computer) as the etalon signal, see Fig. 8.

A two-mode co-propagating collinear CaMoO$_4$ crystalline cell was characterized by a crystal length $L = 4.4$ cm along the [100]-axis, an acoustic velocity $V = 2.95 \cdot 10^5$ cm/s for the shear elastic mode whose displacement vector is oriented along the [001]-axis. The continuous-wave beam at a dark-red light wavelength of $\lambda = 671$ nm (the output optical power ~ 40 mW) had been chosen, first,

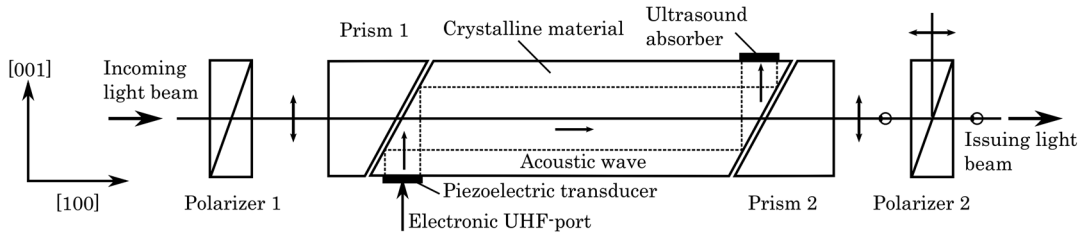**Fig. 8** Schematic arrangement of the experimental set-up.

Fig. 9 Scheme of the co-propagating collinear CaMoO$_4$-cell providing the traveling-wave regime of interaction between the pumping light beam and the continuous-wave lossless acoustic beam.

to minimize the controlling acoustic wave frequency down to about 35 MHz in a view of realizing as close as possible "almost lossless" regime for the propagation of acoustic beam through the CaMoO$_4$ crystalline cell, and second, to just keep the visible range of operation with light beams simplifying the experimental conditions of observations. Thus, the light beam at $\lambda = 671$ nm with the output optical power ~ 40 mW was used as an optical pump during the experiments providing the traveling-wave regime of interaction between the pumping light beam and the acoustic wave. The first polarizer was precisely aligned in correspondence with the optical axes of a crystal in a cell. As the optical pump and the continuous-wave acoustic wave interacted, already two orthogonally polarized light beams, incident and signal ones, passed through a cell. The second polarizer gave us an opportunity to be aligned in correspondence with the polarization of the signal beam and to extract the output optical signal, see Fig. 9.

Then, one can restrict oneself by a maximal level $P \leq 0.5$ W/mm^2 of acoustic power density, which is conditioned by the absolute acoustic power magnitude of about 2 W and the acoustic beam cross section of about 4 mm^2 in the chosen collinear acousto-optical cell. Consequently, one can calculate that $\sigma \leq 2$ cm^{-1}. These estimations demonstrate that the above-noted limitations on both the needed acoustic power density $P_1 \approx 0.233$ W/mm^2 and the parameter $\sigma_1 \approx 0.714$ cm^{-1} lie in the frames of accessible value, while similar parameters P_2 and σ_2 for the second point of collapsing the resolution are beyond these frames.

8 Discussion and Conclusive Remarks

The nonlinear dynamics of varying the transition functions of the optical filter under consideration has been sequentially followed during our experiments as the acoustic power density of the finite amplitude grows. A few examples of the corresponding digitized oscilloscope traces are shown in Fig. 10.

Now, let us discuss this set of oscilloscope traces for the scattered light component intensity $|C_1|^2$ detected during the experiments with the collinear CaMoO$_4$ crystalline cell and estimated at the level 0.4055 conditioned by the Rayleigh criterion. All these traces can be easily interpreted in terms of the above-developed theory taking into account that the first trace in Fig. 10(a) reflects the filter transition function inherent in almost the regime with infinitely small amplitude of the controlling acoustic signal due to the dimensionless value $\sigma L = 0.21$ is very close to zero. This value (which is non-zero, in fact) had been taken as an example to show rather adequately conventional representation for the transition function width or, what is

the same, the filter frequency resolution, being close to $\delta f \approx V/L \approx 68.44$ kHz, as well as to have a chance for identifying the output response whose relative intensity is small enough, i.e., even less then 5%. The second and third traces, peculiar to $\sigma L \approx 1.0$ and $\sigma L \approx \pi/2$ are presented in Fig. 10(b) and 10(c), respectively. From a viewpoint of widely used acousto-optic approach, they can be considered as a natural testimony of growing the relative intensity of the output optical signal up to 0.715 and ~ 1.0 under action of the increasing acoustic power density. They both exhibit the optical resolution of more or less the same order, which varies slightly from the above-mentioned 68.44 kHz to $\delta f \approx 65.84$ kHz and $\delta f \approx 61.45$ kHz, respectively. Such a conclusion looks rather plausible within quasi-linear approximation for the transition function as well as in the course of possible measurements in the frequency domain with not enough accuracy. Nevertheless, further increase of the acoustic power density, depicted by the traces with $\sigma L \approx 2.0$ and $\sigma L \approx 2.5$ in Fig. 10(d) and 10(e), is able to demonstrate step-by-step that the existing specific acousto-optical nonlinearity leads to squeezing the transition function or to improving the frequency resolution to $\delta f \approx 56.24$ kHz and $\delta f \approx 46.14$ kHz, respectively. This process is accompanied by decreasing the relative intensity of the output optical beam down to about 0.82 and 0.35 in the so chosen points. Finally, the last trace, Fig. 10(f), illustrates obviously nonlinear process of squeezing the transition function or improving the frequency resolution in the vicinity of the first point $\sigma L = \pi$ of a collapse. Namely the value $\sigma L \approx 3.0$ has been taken to have an opportunity for revealing the transition function characterized by $\delta f \approx 22.86$ kHz whose relative intensity becomes already dramatically small and does not exceed 2%.

Thus, one can conclude that we have revealed nonlinear squeezing of the transition function inherent in the collinear acousto-optical interaction under condition of the simplifying approximation of lossless (or low-loss) propagation for the acoustic waves. This nonlinear effect can be interpreted also as improving the spectral and frequency resolution peculiar to the collinear acousto-optical filter operated by the controlling acoustic waves of the finite amplitude. Rather adequate theory of this effect has been developed analytically and illustrated via the corresponding computer simulations. In particular, a periodicity for the nonlinear squeezing of the transition function, which includes a set of points as its collapses originating periodically, has been found and estimated. It has been shown that the first period of similar collapsing exhibits the best relation between the width and magnitude of the squeezed transition function from the viewpoint of practical application. Then, the needed estimations have been performed for the collinear interaction, which made it possible to choose a dark-red light laser beam,
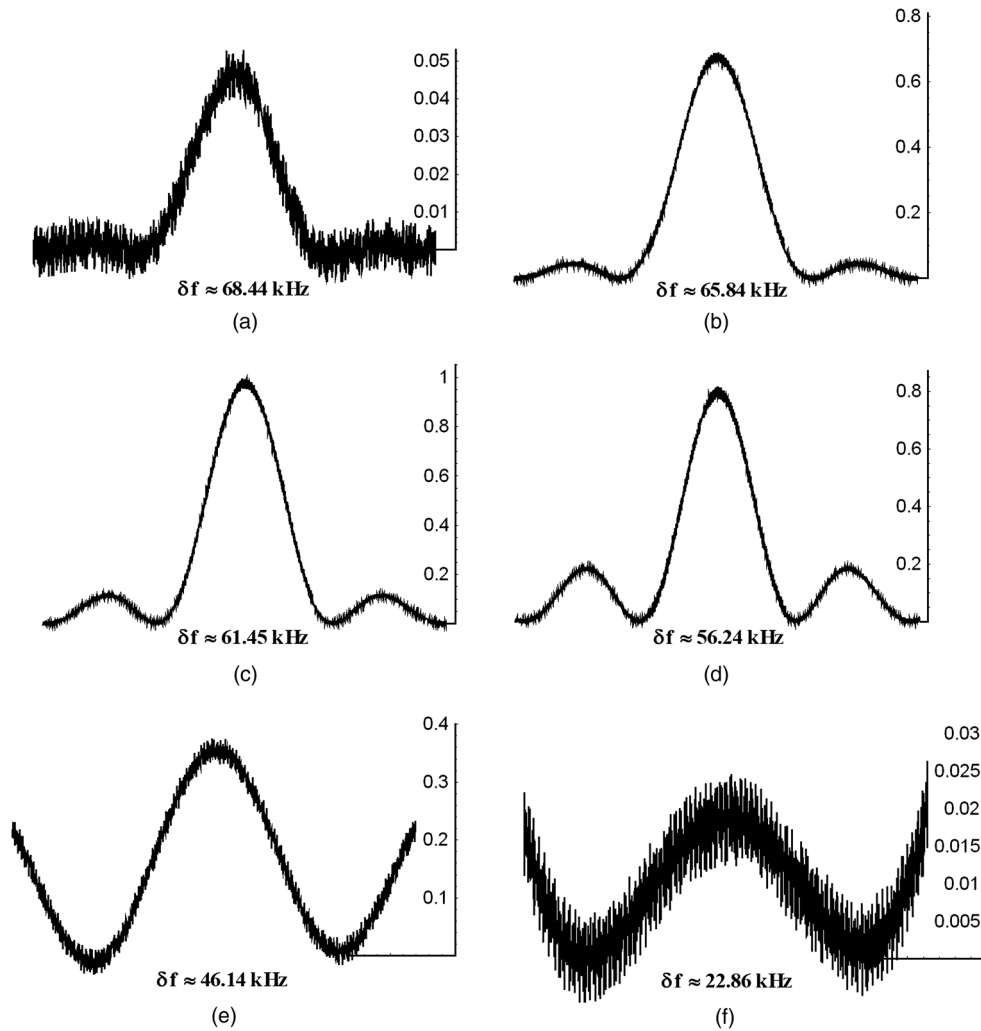
Fig. 10 The digitized oscilloscope traces for the scattered light intensity $|C_1|^2$ observed at the output of the collinear $CaMoO_4$ cell at the carrier acoustic frequency of $\sim$37.3 MHz and estimated at the level 0.4055. Reshaping the transmission function is followed at the same optical pump in variable scales: (a) $\sigma L = 0.21$, $P \approx 0.00104[W/mm^2]$; (b) $\sigma L \approx 1.0$, $P \approx 0.0236[W/mm^2]$; (c) $\sigma L \approx \pi/2$, $P \approx 0.0582[W/mm^2]$; (d) $\sigma L \approx 2.0$, $P \approx 0.0944[W/mm^2]$; (e) $\sigma L \approx 2.5$, $P \approx 0.148[W/mm^2]$, and (f) $\sigma L \approx 3.0$, $P \approx 0.223[W/mm^2]$.

lying still in the visible range, and a low-frequency acoustic wave, providing its almost lossless propagation, in a $CaMoO_4$ single crystal. Finally, the results of our experiments illustrating the nonlinear squeezing of the transition function with lossless propagation of acoustic waves in the collinear calcium molybdate crystalline cell have been presented and briefly discussed.

References

1. J. L. Bertaux et al., "SPICAM: Studying the global structure and composition of the martian atmosphere," in *European Space Agency; SP-1240 Mars Express: A European mission to the red planet*, A. Wilson, Ed., ESA Publications Division (2004).
2. J. L. Bertaux et al., "SPICAV on venus express: three spectrometers to study the global structure and composition of the venus atmosphere," *Planet. Space Sci.* **55**(12), 1673–1700 (2007).
3. R. W. Dixon, "Acoustic diffraction of light in anisotropic media," *IEEE J. Quant. Elect.* **QE-3**(2), 85–93 (1967).
4. S. E. Harris, S. T. K. Nich, and R. S. Fiegelson, "$CaMoO_4$ electronically tunable optical filter," *Appl. Phys. Lett.* **17**(5), 223–225 (1970).
5. I. C. Chang, "Tunable acousto-optic filter utilizing acoustic beam walk-off in crystal quartz," *Appl. Phys. Lett.* **25**(6), 323–324 (1974).
6. J. A. Kusters, D. A. Wilson, and D. L. Hammond, "Optimum crystal orientation for acoustically tuned optical filters," *J. Opt. Soc. Am.* **64**(4), 434–440 (1974).
7. E. T. Aksenov, N. A. Esepkina, and A. S. Shcherbakov, "Acousto-optical filter with a $LiNbO_3$-crystal," *Tech. Phys. Lett.* **2**(3), 83–84 (1976).
8. J. D. Feichtner, M. Gottlieb, and J. J. Conroy, "Tl^3AsSe_3 noncollinear acousto-optic filter operation at 10 μm," *Appl. Phys. Lett.* **34**(1), 1–3 (1979).
9. V. I. Balakshy, V. N. Parygin, and L. I. Chrkov, *Physical Principles of Acousto-Optics*, Radio I Svyaz, Moscow (1985).
10. A. Korpel, *Acousto-Optics*, 2nd ed., Marcel Dekker, New-York (1997).
11. F. T. S. Yu, *Introduction to Information Optics*, Academic Press, San Diego (2001).
12. A. S. Shcherbakov and A. Aguirre Lopez, "Shaping the optical components of solitary three-wave weakly coupled states in a two-mode waveguide," *Opt. Express* **11**(14), 1643–1649 (2003).
13. A. S. Shcherbakov and A. Aguirre Lopez, "Binary encoded modulation of light based on collinear three-wave acousto-optical weakly coupled states," *J. Opt. A: Pure and Appl. Opt.* **5**, 471–477 (2003).
14. Yu. I. Sirotin and M. P. Shaskolskaya, *Fundamentals of Crystal Physics*, Mir Publishers, Moscow (1982).
15. V. G. Dmitriev, G. G. Gurzadyan, and D. N. Nikogosyan, *Handbook of Nonlinear Optical Crystals*, 3rd ed., Springer, Berlin (1999).
16. A. A. Blistanov, *Crystals for Quantum and Nonlinear Optics*, 2nd ed., MISIS, Moscow (2007).
17. D. A. Pinnow, "Guidelines for the selection of acousto-optic materials," *IEEE J. Quant. Elect.* **QE-6**, 223–238 (1970).
18. M. P. Shaskolskaya, Ed., *Acoustical Crystals Handbook*, Nauka Publishers, Moscow (1988).

Alexandre S. Shcherbakov obtained his MSc and PhD degrees in radiophysics from St. Petersburg State Technical University in 1972 and 1977, respectively. He joined the staff of this university in 1972, where he was the head of Nonlinear Optics Laboratory until 1999. From 2000 he is visiting the INAOE, Mexico. For many years, he has focused on studying various nonlinear phenomena and optical solitary waves in crystals, fibers, and semiconductor structures as well as on their applications to a high-bit-rate processing of both analog and digital data.

Sergey A. Nemov obtained his MSc and PhD degrees in semiconductors & dielectrics from St. Petersburg State Technical University in 1972 and 1978, respectively. He joined the staff of this university in 1972, and from 2000, he was the head of Applied Physics & Solid State Optics Department. Now, he is a professor in the Physical Chemistry & Advanced Material Technology Division. For many years his interests lie in studying optical and photo-electrical properties of solids, semiconductors, and disordered systems.

Adán Omar Arellanes is currently with the National Institute of Astrophysics, Optics, and Electronics (INAOE), Mexico as an MSc student. He received his BSc degree from Autonomous University of Nuevo Leon (2007). His research interests include acousto-optics and nonlinear optics. He is a student member of the SPIE and OSA.